Development of a Reliable Method for Orbit Segmentation & Measuring

Matthias Becker, Karl-Ingo Friese, Franz-Erich Wolter
Welfenlab, Leibniz University Hanover, Hanover, Germany

Nils-Claudius Gellrich
Dep. of Oral and Maxillofacial Surgery, Hanover Medical School, Hanover, Germany

Harald Essig
Dep. of Oral and Maxillofacial Surgery, University Hospital of Zürich, Zürich, Switzerland

***Abstract*—Injuries of the bony orbit, which contains the eye, not only have aesthetic implications but also impair stereoscopic vision. Different techniques are used for surgical treatment. In this work we will present a tool that allows the reliable segmentation of the reconstructed and the unaffected orbit. For this we present a novel anterior closing that follows the clinical understanding of anatomy. To assist in the post-surgical evaluation, we suggest parameters with respect to clinically relevant regions (orbital floor, medial wall) and demonstrate a method to automatically determine them. We evaluate our methods on three clinical cases.**

I. Introduction

Physical injuries in the area of the human face, especially close to the eye, are considered to be particularly distressful. In our perception, the face, like no other body part, is connected to the identity of a person. Injuries through accidents, violence or tumors, that affect the position of the eye, not only have an aesthetic impact but can also impair the functionality, e.g. stereographic vision. Different surgical treatments exist to restore the eye to its original position. The human eye is held by a bony structure, the bony orbit. In this work, we propose a method to evaluate the surgical outcome.

One of the main tasks in 3D medical imaging is the identification of structures, e.g. organs, bones or muscles, known as segmentation. Commonly orbit segmentation is performed manually by tracing the orbit boundaries on each computed tomography (CT) image slice. We will present a tool that allows the automatic segmentation and the comparative analysis of this bony orbit. Our proposed method will address two issues:

1) A reliable segmentation of the reconstructed and non-affected orbit and a
2) 3D shape analysis of both segments with a focus on clinically relevant regions (orbital floor, medial orbital wall).

Our segmentation method has to deal with different imaging modalities: Computer Tomography (CT) and Cone Beam CT (CBCT). It should work similarly on reconstructed and non-affected orbits, and be independent from the reconstruction material. One challenge in orbit segmentation is its geometrical definition, since the anterior closing is not well defined. Additional openings exist in the surrounding bone structures (foramina) and in the implanted titanium mesh. Both aspects will be addressed through a model based segmentation method using a rough manual positioned mean orbit model which will then be used for an automated evolution algorithm.

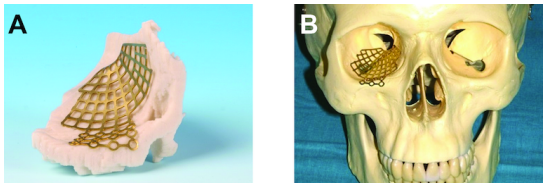

Fig. 1. Patient-Specific Orbital Reconstruction

II. Bony Orbit

The orbital content such as eye globe and its appendages is located in and protected by the bony orbit, which is a four-sided pyramidal cavity. The complex configuration is clinically divided into orbital roof, medial and lateral orbital wall and orbital floor. Especially in the posterior part of the orbit (apex of the pyramid) there are foramina for afferent and efferent cranial nerves including the optic nerve.

Due to the varying orbital wall thickness, the very thin orbital floor and medial orbital wall are typically fractured in orbital traumata. The majority of orbital wall fractures require orbital reconstruction to support the globe position and restore volume and shape of the orbit. Repositioning of dislocated bony fragments is often not feasible and therefore the procedure is more related to a true-to-original reconstruction of the orbital walls. Different reconstruction materials are available. Resorbable membranes are widely used in minor defects, while form-stable titanium implants are inserted in major defects. The decision of the extensiveness of the orbital reconstruction is still highly controversial. However, the postulation to reconstruct true-to-original is beyond controversy. Independent of the used reconstruction material the orbital shape and volume should be identical to the mirrored contralateral orbit.

Figure 1 shows the approach used at the MHH: A titanium mesh is moulded as an implant on a patient-specific stereolithographic (STL) model, based on the mirrored non-affected contralateral orbit (A). (B) shows a demonstration of the desired implant position using a standard skull.

Figure 2 demonstrates the technique for orbital floor fractures: (A) shows a scheme of a typical defect of the orbital floor that often causes inherniation of orbital content, the arrow (B) shows a defect area in the anterior orbital floor. (C)

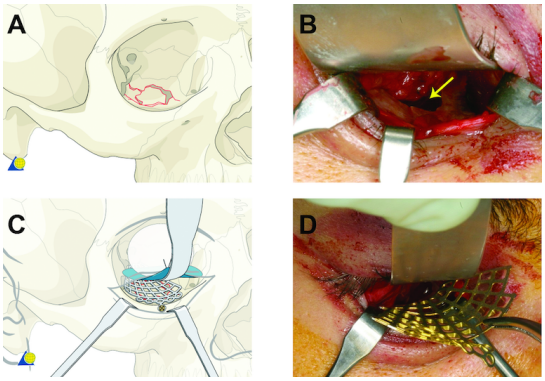

Fig. 2. Surgical technique in orbital floor fracture

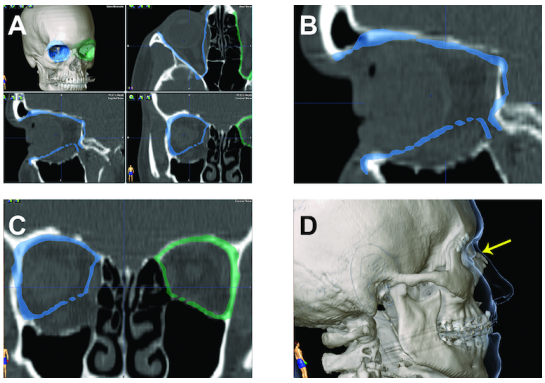

Fig. 3. Inadequate Result after Orbital Reconstruction with Resorbable Membrane

illustrates the scheme of orbital reconstruction with titanium mesh implants, and the patient-specific titanium implant is inserted in (D).

Figure 3 shows an inadequate result. The affected orbit is considerably enlarged and results in a malposition of the eye globe with double vision. The analysis of the CT data set with multiplanar view is shown in (A): the segmentation of the non-affected orbit (green) and mirroring of this template to the affected side (blue). The sagittal view (B) shows a hammock-like configuration of the affected side and virtual mirroring of the non-affected side demonstrates the desired true-to-original position of the orbital floor. The Coronal view (C) demonstrates the enlarged right (patient-side) orbit. The contour (D) of the periorbital soft tissue demonstrates the posterior position due to the enlarged orbit and malposition of the eye globe.

III. Literature Overview

A. Research on the Bony Orbit

First publications about measurement procedures start in 1936. Breitinger et al. [1] closed the orbital foramina and filled the orbital cavity with mustard seeds. The anterior closing was defined as the most anterior bony rim. According to this definition, Bite [2] described in 1985 first digital measurements using computed tomography data sets with comparable results. While some authors specify a vertical plane through the most anterior points of the lateral orbital walls [3] for the anterior closing, most authors prefer an anterior closing which is defined by the anterior bony rim of the orbit [2], [4]. This preferred method is independent of the contralateral anatomy.

Recent publications for orbital volume and shape analysis are mainly focused on construction of pre-formed reconstruction materials [5] and on secondary reconstruction after inadequate surgical primary intervention [6]. Currently, there is no orbital measurement tool which allows a post-operative quality control.

B. Deformable Models and Orbit Segmentation

The usage of medical imaging opens a new perspective on many medical problems. The process, described in [7], begins with image acquisition, continues on image enhancement and leads to segmentation. The manual creation of segments is an elaborate task whose time consumption increases with image resolution. (Semi-)Automatic methods are being developed to reduce creation time and to increase the accuracy of the results. Simple approaches like thresholding of intensities or region growing provide good results but fail on complex shapes or poor image modalities that are common in medical imaging (e.g. due to efforts to decrease the radiation dose).

Deformable models were introduced by Kaas et al. [8]. Bredno et al. [9] describe a general deformable model for multiple dimensions. Model based segmentation approaches start from the usage of snakes by Klinski [10]. Kleiner et al. [11] have extended it to deformable models and Nystrm et. al. [12] further improved it and added haptic interaction capabilities. They all reach satisfactory results using CT images. Lamecker et al. present in [13] a Statistical Shape Models (SSM) to model shape variety and to allow the robust division of the orbit into six predefined parts. Another approach is using an atlas [14]. Measuring of the orbital volume is possible with all segmentation approaches, an automated determination of more parameters has not been conducted. So far, none of the approaches has been tested with CBCT data.

IV. YaDiV

A. General

YaDiV is an open platform for visualization, segmentation and analysis of (medical) volume data, developed at Welfenlab, University of Hanover [15]. It has many features to visualize or interact with tomographic data (including support of virtual reality hardware). Existing segmentation modules in YaDiV already include region, range, edge detection, atlas based and active contour (based on the level set approach) methods. The development of a model specific approach is usually very time consuming. To overcome this, we use a new sub framework of YaDiV.

B. YaDiV Deformable Model Framework (YDMF)

The YaDiV Deformable Model Framework (YDMF) allows the design of deformable model approaches for new applications. Its core data structure is a highly inter-linked closed triangle mesh, the so called Deformable Model (DM), that is iteratively deformed until it outlines the shape of the desired structure.

The initial mesh should be more or less close to the final outcome and is usually a bit smaller. It can be obtained by

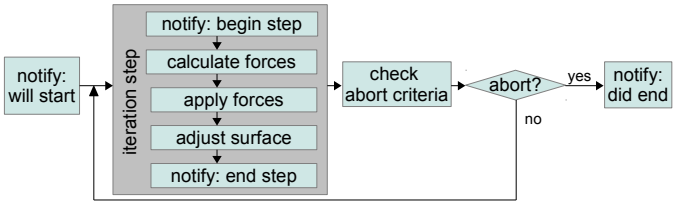

Fig. 4. Evolution process

a manual segmentation of a sufficiently generic real world example, which can be edited with the built-in graphical YaDiV Deformable Model (YDM) editor. With the editor it is also possible to add model-specific meta-information (so called labels), that can be attached to vertices, triangles or edges of the DM. The labels can be used to mark anatomical landmarks or points/curves/areas, whose geometric features should be preserved, e.g. by using modified forces during the mesh evolution.

YDMF uses the structure shown in Figure 4 and consists of the following four main components, that can be used for the rapid development of custom model based approaches.

Forces can be applied to triangles, edges and vertices. If more than one force is used, the forces will be combined before they are applied. Examples are growing-, smoothing- and image-forces.

Surface Adjuster modify the surface and are executed in each iteration after the forces got applied. For example they can be used to ensure a maximum edge length by splitting up edges / triangles to keep the resolution adequate during the expansion.

Abort Criteria are evaluated at the end of each step and abort the iteration process. Examples would be a maximum number of steps or the growing out of a predefined bounding box.

Notifications inform about everything important during the iteration. They get called at the beginning and end of each step as well as after force calculation. For example, they allow interactive visualization, can be used for logging, the export of statistics, or to invoke external systems.

V. Segmentation of the Bony Orbit

The segmentation of the bony orbit is a time consuming task. With modern medical imaging systems resolution increases. A manual segmentation by an experienced physican takes 20-30 minutes. This time increases linearly with higher resolution.

Current methods for automated orbit segmentation all work with Computer Tomography (CT) images, that provide good contrast and a reliable conversion from intensity values to Hounsfield Units (HU). Opposite to this, we tested our approach with CT as well as Cone Beam CT Images (CBCT) images. This new technology replaces the 1D- slices based approach from CT with a 2D-approach. The ray source emits a cone-shaped beam that travels through the patient and is received by a 2D-detector, illustrated in Fig. 5.

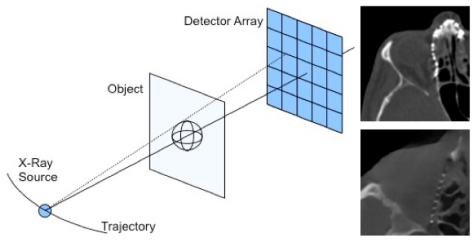

Fig. 5. Working principle of a cone beam CT and the resulting images (bottom) in comparison to CT (top)

CBCT reduces the radiation dose for the patient, but the resulting images are harder to process than CT images: They have lower contrast, high noise and especially for soft tissue there is no well-defined mapping from intensity values to HU anymore. Furthermore, the mapping is not consistent throughout the image. Figure 5 shows a comparison of a CBCT and a CT image.

A. YDMF based Orbit Segmentation

We used the YDMF to implement a YaDiV module for orbit segmentation by making the following adjustments.

1) Forces: We added three forces to evolve the initial model until it reaches its final shape: a general growing force along the normals, a smoothing force (internal forces) and an (external) image force.

The special orbit geometry and its many openings requires a mechanism to prevent the model from leaking through holes (image artifacts, openings for tissue, nerves, etc.). We have found that a Laplacian smoothing provides good results with low computational effort. Since the CBCT images can not be mapped to HU-values, we use only the gradient to calculate the image force. High gradients appear at bones or the titanium mesh, but they may vary depending on parameters during image acquisition.

2) Labels and Surface Adjuster: To exploit prior model knowledge we use the label concept of YDMF. For the anterior closing, we have added an initial path (a set of connected edges) close to the final position in the initial model. We have also asked a physician to mark the orbital floor and the medial wall using triangle labels. By that we can use expert knowledge to detect these structures that are important for analysis.

During the evolution, we put a constraint on the mesh edge length to $3\mathrm{mm}$. Thus our high resolution model fits into all orbital features and its shape is approximately similar to the actual orbit boundary. Any longer edges were automatically split into two edges.

After eachs tep, during refinement, labels may have to be adjusted. If the original edge e was part of the initial path for the anterior closing, the two newly created edges will also belong to the path. If one of the triangles along e was part of the orbital floor or the medial wall, the two replacing triangles will also be part of it.

3) Mesh Evolution: To define an abort criterion as well as to speed up the mesh evolution, we added a mechanism that marks vertices that have reached the equilibrium of forces (meaning they did not move after a given number of steps) as

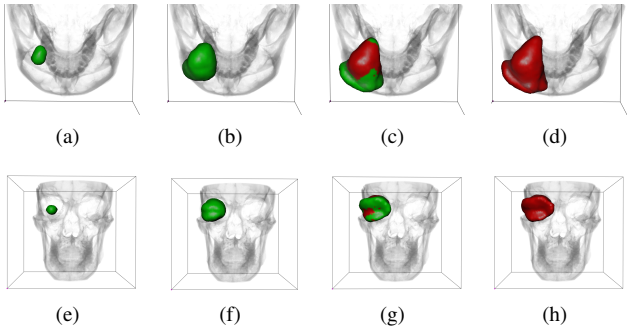

Fig. 6. Mesh evolution from initial model (a), (e) to final result (d), (h) from transversal (first row) and frontal perspective (second row). Green parts evolve, red parts are already fixated.

fixed. We have an abort criterion to 99.5% of fixed vertices. We have also limited the number of steps. Figure 6 shows the evolution of a mesh from an initial model to its final shape.

B. Anterior Closing

Finding a good anterior closing is a complex task. Even physicians use several different approaches to define the anterior closing. Due to the working principle of the eye, there is no natural well-defined closing. In manual segmentation, in each slice the orbit rim on the zygomatic bone is connected to the maxilla bone with a line, which is not a practical solution for automated systems. Several approaches have been proposed that define limiting planes based on anatomical landmarks:

1) Different Closing Approaches: The initialization of our models relies on the manual determination of centers of the eye globes (EGCs). These points can be combined with the given knowledge of the orientation of the head to insert a single plane (see Fig. 7(a)) that acts as a closing. To handle the lateral leaking, this approach can be extended to three planes with a third point that is close to the nose tip. This simple approach, seen in Fig. 7(b), prevents lateral leaking, offers comparable volumes, but its medical sensibility is limited.

Other approaches work with manually placed anatomical landmarks. An automated placing has been shown 2008 by Kleiner in [11]. Along the optical axis a plane is moved towards the eye. Once a point on that plane hits the bone, it is used as a landmark and surrounding angles get excluded. This process is continued until three points are found. They define a plane, illustrated in Fig. 7(c). Another approach uses the zygomatic bone. Both eye globe centers and a caudal pointing vector form a plane that is searched towards the eye from the outer sites for bone structures (the zygomatic bone, the medial area has been excluded to avoid finding the nasal bone). Once a point on each zygomatic bone is found, a closing plane, see Fig. 7(d), can be created together with the previously used frontal pointing vector.

2) New: Convex Closing: Given a good parametrization, we have found that the model tends to grow out of the bony orbit in the anterior part and into the facial tissue. Especially in images taken short after an operation this tissue is swollen and easy to reach, as shown in Fig. 8(a). Along the optimal border of the orbit the model is concave. This path is used to create a local convex object and forms the closing path. We

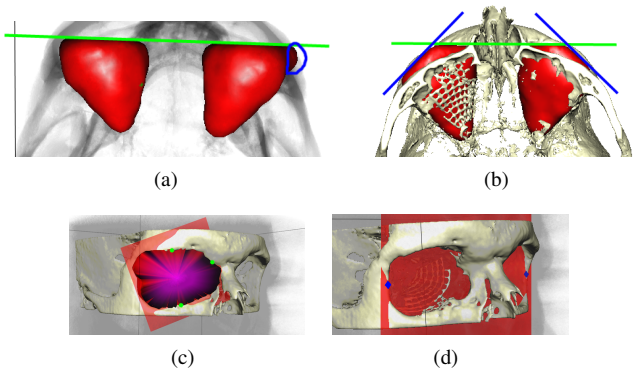

Fig. 7. Different approaches for the Anterior Closing

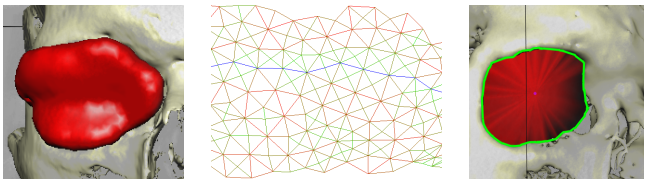

Fig. 8. Anterior Closing of the swollen model, (a) the neighborhood around an inital path (b) is evaluated (green: small weight, red: high weight, blue: final path) to find an optimal closing (c).

have defined a path in the initial model using YDMF labels. After the mesh evolution, this path still lies close to the desired contour.

Around this initial path we define a search area for the optimal path. To find it, we assign weights to the edges which are based on two factors: 1. Edges whose vertices do not touch bones get a higher weight and 2. Vertices that are at a convex position of the shape also distribute higher weight to the connected edges.

Having assigned weights, as shown in Fig. 8(b), we can use a simple optimization approach to calculate the optimal path. Once we have found the optimal path, we remove all triangles in front of it and close the surface by adding a new vertex v_c in the centroid of the optimal path. The resulting closing is shown in Fig. 8(c).

3) Comparison of approaches: We used three major criteria for a qualitative assessment of an anterior closing, as shown in Table I.

Medically sensible: The achieved volume has to be sensible from the perspective of a physician. Every approach needs to fulfil this. A well defined, reproducible approach is useless if it does not reflect the anatomy of the orbit.

Comparability: Each approach should define the anterior closing in a way that allows a reliable comparison of both orbits.

Lateral leaking: During the evaluation of different existing approaches, we found some of them to produce lateral leaking.

The results clearly show that there are only four candidates. The three layer approach shows a partially sensible volume and fulfills the other two criteria but does not satisfy clinical needs that go beyond prototyping. All manual approaches can

TABLE I. COMPARISON OF CLOSING APPROACHES

Approach	medically sensible volume	comparability of volumes	prevents lateral leaking
convex border	yes	yes	yes
single layer	no	yes	no
triple layer	partially	yes	yes
three landmarks	no	no	no
zygomatic bone connection	no	yes	yes
manual landmarks	possible	possible	possible
sphere	no	yes	yes
manual border	yes	yes	yes

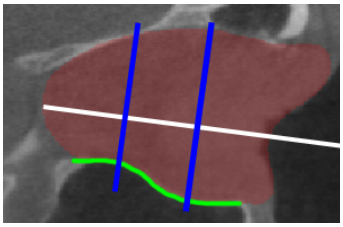

Fig. 9. From an axial perspective the s-shape of the bony orbit is highly recognizable

deliver good results but depend heavily on user input, limiting reproducibility and increasing effort. This lead us to the convex border approach which meets all our requirements and requires no user interaction.

VI. ORBIT ANALYSIS AND COMPARISON

A. Parameter Selection

Assessing the outcome of an operation is crucial for further improvements. A common symptom of fractures of the bony orbit is an increased orbit volume leading to a dislocated globe and it is important to restore its initial position. Therefore the first parameter for comparison is the orbit volume.

The titanium mesh used for replacing the fractured bone structures should be formed as close to the bone original shape as possible. The contralateral orbit is used as a template. The angle between orbital floor and medial wall, where the fractures are located, plays an important role for the comparison. For robust calculation, we must consider the "S"-like shape of the orbital floor. Therefore we divide the orbit into an anterior, medial and posterior part, as seen in Fig. 9, and calculate their angles separately.

Finally, we want to perform a comparison of the whole shape and to calculate the distance between both orbit shapes, after a registration has been performed.

B. Parameter Determination

The calculation of the orbital volume is performed in voxel representation. The YDMF already offers the capability to transform a surface model into a discrete voxel model. Using the voxel size (from Dicom), we can calculate the volume.

The calculation of the angles between orbital floor and medial wall can be divided into two parts: 1. the determination of the division and 2. the actual angle calculation.

Because of the complex orbital anatomy, we used prior expert knowledge and asked a physician to mark both areas on the initial model using the built-in labeling mechanism of the YDM editor. In a first step we refine and smooth the border between orbital floor and medial wall. The backmost point of the model and the centroid v_c of the optimal path of the anterior closing describe a good approximation of the optical axis. After calculating the foremost and backmost points of the orbital floor we can put separation planes along the optical axis to get the anterior, medial and posterior third of the orbital floor and medial wall. For each third we average the floors and medial walls triangle normals and calculate the angle between them.

C. Orbit Comparison

In addition to the previously described parameters we want to compare the complete shape of both orbits. For this, we align both shapes using their centroid. To refine the results, we use a rigid best-neighbor registration with translation and rotation only. We then calculate the distance between the shapes by going through all vertices of the left orbit and find the distance to the closest point on the surface of the right shape. If we have these results for all vertices we can calculate several statistical metrics like mean, median, min and max-differences.

VII. EVALUATION

To evaluate our segmentation and closing approach we have tested and compared our framework with six orbits from three data sets. In each data set one orbit was non-affected and the other one was reconstructed using a titanium mesh. All data sets were acquired using a PaX-Zenith 3D by VaTech CBCT with a voxel size of $0.3 \times 0.3 \times 0.3\mathrm{mm}$.

In our first test we segmented the orbit and applied our closing. We compared the resulting segment with the manual segmentation of an expert, using the Dice Similarity Coefficient (DSC), which takes the overlap into consideration when comparing two volumes X,Y: $DSC = \frac{2|X \cap Y|}{|X|+|Y|}$. Table II shows the results. To measure the intra-individual variation of the manual segmentation, we had a data set segmented manually twice. The results were a DSC of 0.9166 and 0.9474 for the right and the left orbit.

TABLE II. EVALUATION OF THREE DATA SETS FOR DCS AND VOLUME, * INDICATES RECONSTRUCTED ORBITS.

Data set	DSC	automatic volume (ml)	manual volume (ml)
1, left	0.9105	27.6424	29.7948
1, right*	0.8737	23.1951	24.7241
2, left	0.9125	28.6339	30.2125
2, right*	0.9056	27.1625	29.4520
3, left*	0.8641	26.1475	30.1177
3, right	0.8221	24.4484	27.8623

Notable is the volume difference of $2.48 \pm 0.99\mathrm{ml}$ between manual and automatic segmentation of our three data sets, especially in data set 3. We have found three major reasons. In the manual segmentation the superior orbital fissure and the optic canal have been segmented in great detail. Our approach focuses on the orbital parts that were reconstructed and therefore prevents the model from growing into small structures in the posterior part of the orbit. An example of the different segmentation results on the posterior part of the orbit is shown in Fig. 10(a). We also found out that the manual segmentation often contains parts of the bone. The automatic

segmentation prevents entering bone and therefore has less volume, visible in Fig. 10(b) and 10(c). The third problem for comparison were the different closing approaches. The manual segmentation performed a slice-wise closing by connecting the zygomatic and the maxillary bone. Our approach detects the rim globally and closes the segment with an additional point in the centroid, as shown in Fig. 10(d).

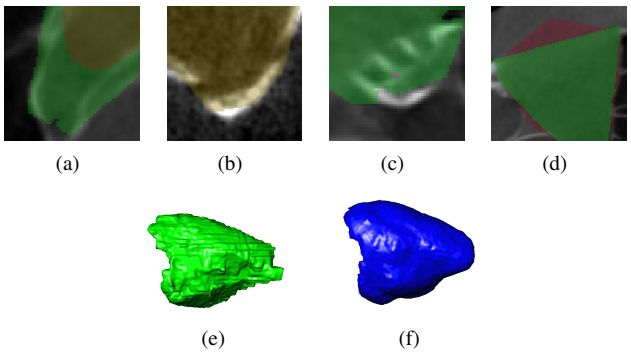

Fig. 10. (a) Different segmentation in the optic canal (green manual, yellow automatic), manual segmentation inside bone (b) and titanium mesh (c), (d) differences from manual (green) and automatic (red) closing. (e) and (f) show the difference between slicewise and global approaches.

Additionally we have determined the angles between orbital floor and medial wall for the anterior, medial and posterior third of the orbit. They are listed in Tab. III. We see only small differences between left and right orbit in the medial and posterior third, whereas in the anterior third the differences are too high.

TABLE III. ANGLE MEASUREMENT RESULTS

Data set	ant. angle	med. angle	post. angle
1, left	78.2	69.7	69.7
1, right*	84.4	77.2	75.2
2, left	121.1	75.5	68.7
2, right*	85.6	79.9	75.7
3, left*	98.5	87.5	87.6
3, right	80.2	83.7	84.4

A clearly visible result in the comparison between manual and automatic segmentation is the smooth surface of the automated approach. As a manual segmentation works slice-wise it cannot make use of the slices above and below like our three-dimensional approach, leading to a discontinuous surface as seen in Figure 10(e) and (f).

VIII. SUMMARY AND OUTLOOK

In this work, we have presented an approach for orbit segmentation and the measurement of shape properties. For segmentation we have used the deformable model framework YDMF of YaDiV. We have introduced a new approach to construct the anterior closing by creating a local convex cutting polygon at the swelling part after the mesh evolution. To assist in clinical evaluation or orbit reconstruction surgery, we determine three parameters comparing non-affected and reconstructed orbit: orbit volume, angle between floor and medial wall and the distance between both shapes. Our approach has been evaluated with clinical data.

Deformable models provide a good foundation for the successful segmentation of the bony orbit. Especially in data sets with poor image quality, our approach shows potential for optimization. To overcome small problems like artefacts or non-visible bones, attraction and rejection points could be placed by the user to improve segmentation results. The presented method depends on the imaging parametrization (coil voltage, currents) and requires one time adjustments which could be reduced in future work. More extensive use of prior knowledge could lead to reduced numbers of user interactions.

ACKNOWLEDGMENT

We would like to thank the AO Foundation, Davos, Switzerland for supporting this work. Some illustrations in this work are reproduced with kind permission of the AO Foundation.

REFERENCES

[1] E. Breitinger, "Zur Messung der Schädelkapazität mit Senfkörnern," *Anthropol Anz*, vol. 13, p. 140, 1936.

[2] U. Bite, I. T. Jackson, G. S. Forbes, and D. G. Gehring, "Orbital volume measurements in enophthalmos using three-dimensional ct imaging." *Plastic and Reconstructive Surgery*, vol. 75, no. 4, pp. 502–508, 1985.

[3] R. Whitehouse, M. Batterbury, A. Jackson, and J. Noble, "Prediction of enophthalmos by computed tomography after 'blow out' orbital fracture." *Br J Ophthalmol*, vol. 78, no. 8, pp. 618–20, 1994.

[4] Y. Ji, Z. Qian, Y. Dong, H. Zhou, and X. Fan, "Quantitative morphometry of the orbit in chinese adults based on a three-dimensional reconstruction method." *J Anat*, vol. 217, no. 5, pp. 501–6, 2010.

[5] M. Metzger, M. Gissler, M. Asal, and M. Teschner, "Simultaneous cutting of coupled tetrahedral and triangulated meshes and its application in orbital reconstruction," *International Journal of Computer Assisted Radiology and Surgery*, vol. 4, pp. 409–416, 2009.

[6] N.-C. Gellrich, A. Schramm, B. Hammer, S. Rojas, D. Cufi, W. Lagréze, and R. Schmelzeisen, "Computer-assisted secondary reconstruction of unilateral posttraumatic orbital deformity." *Plast Reconstr Surg*, vol. 110, no. 6, pp. 1417–29, 2002.

[7] A. P. Dhawan, *Medical Image Analysis*, second edition ed., L. Hanzo, Ed. John Wiley & Sons, Hoboken, New Jersey, 2011.

[8] M. Kass, A. Witkin, and D. Terzopoulos, "Snakes: Active contour models," *International Journal of Computer Vision*, vol. 1, pp. 321–331, 1988, 10.1007/BF00133570.

[9] J. Bredno, T. M. Lehmann, and K. Spitzer, "A general discrete contour model in two, three, and four dimensions for topology-adaptive multichannel segmentation," *IEEE Transactions on Pattern Analysis and Machine Intelligence*, vol. 25, pp. 550–563, 2003.

[10] S. von Klinski, "Modellbasierte Auswertung von dreidimensionalen Schnittbilddaten der Orbita," Ph.D. dissertation, Freie Universitt Berlin, 2001.

[11] M. Kleiner, "Ein routine-integrierbares Planungswerkzeug zur operativen Rekonstruktion der Orbita," Master's thesis, RWTH Aachen Universittsklinikum, 2008.

[12] I. Nystrm, J. Nysj, and F. Malmberg, "Visualization and haptics for interactive medical image analysis: Image segmentation in craniomaxillofacial surgery planning," in *Visual Informatics: Sustaining Research and Innovations*, 2011, vol. 7066.

[13] H. Lamecker, L. Kamer, A. Wittmers, S. Zachow, T. Kaup, A. Schramm, H. Noser, and B. Hammer, "A method for the three-dimensional statistical shape analysis of the bony orbit," *Proc. Computer Aided Surgery around the Head*, pp. 94–97, 2007.

[14] S. Panda, A. J. Asman, S. P. Khare, L. Thompson, L. a. Mawn, S. a. Smith, and B. a. Landman, "Evaluation of multiatlas label fusion for in vivo magnetic resonance imaging orbital segmentation," *Journal of Medical Imaging*, vol. 1, no. 2, p. 024002, Jul. 2014.

[15] K.-I. Friese, P. Blanke, and F.-E. Wolter, Friese, "YaDiV – an open platform for 3D visualization and 3D segmentation of medical data," *The Visual Computer*, vol. 27, pp. 129–139, 2011.